Effect of 8-Oxo-1,N^6-Ethenoadenine Derivatives on the Activity of RNA Polymerases from SARS-CoV-2 and *Escherichia coli*

Ivan V. Petushkov[1,2,a]*#, Andrey V. Aralov[3,4#], Igor A. Ivanov[3,5], Mikhail S. Baranov[3,6], Timofey S. Zatsepin[7], and Andrey V. Kulbachinskiy[1,2,b]*

[1]*National Research Centre "Kurchatov Institute", 123182 Moscow, Russia*

[2]*Institute of Gene Biology, Russian Academy of Sciences, 119334 Moscow, Russia*

[3]*Shemyakin–Ovchinnikov Institute of Bioorganic Chemistry, Russian Academy of Sciences, 117997 Moscow, Russia*

[4]*RUDN University, 117198 Moscow, Russia*

[5]*Organicum LLC, 127486 Moscow, Russia*

[6]*Pirogov Russian National Research Medical University, 117997 Moscow, Russia*

[7]*Faculty of Chemistry, Lomonosov Moscow State University, 119991 Moscow, Russia*

[a]*e-mail: telomer1@rambler.ru*   [b]*e-mail: avkulb@yandex.ru*

Abstract—Bacterial and viral RNA polymerases are promising targets for the development of new transcription inhibitors. One of the potential blockers of RNA synthesis is 7,8-dihydro-8-oxo-1,N^6-ethenoadenine (oxo-εA), a synthetic compound that combines two adenine modifications: 8-oxoadenine and 1,N^6-ethenoadenine. In this study, we synthesized oxo-εA triphosphate (oxo-εATP) and showed that it could be incorporated by the RNA-dependent RNA polymerase of SARS-CoV-2 into synthesized RNA opposite template residues A and G in the presence of Mn^{2+} ions. *Escherichia coli* RNA polymerase incorporated oxo-εATP opposite A residues in the template DNA strand. The presence of oxo-εA instead of adenine in the template DNA strand completely stopped transcription at the modified nucleotide. At the same time, oxo-εATP did not suppress RNA synthesis by both RNA polymerases in the presence of unmodified nucleotides. Therefore, the oxo-εA modification significantly disrupts nucleotide base pairing during RNA synthesis by RNA polymerases of different classes, and the corresponding nucleotide derivatives cannot be used as potential antiviral or antibacterial transcription inhibitors.

DOI: 10.1134/S0006297924120149

Keywords: modified nucleobases, RNA polymerase, transcription, transcription inhibitors, SARS-CoV-2

INTRODUCTION

Derivatives of natural nitrogenous bases, nucleosides, nucleotides, and nucleic acids are widely used in both fundamental research and development of therapeutic agents, since modifications can lead to the emergence of novel properties of these compounds compared to their natural analogues. The re- cent pandemic caused by the RNA virus SARS-CoV-2 has stimulated the search for new nucleoside inhibitors of viral RNA-dependent RNA polymerase (RdRp) and demonstrated the need for the development of effective drugs in the event of emergence of resistant strains and/or new viruses. One possible candidate inhibitor of RdRp is 7,8-dihydro-8-oxo-1,N^6-ethenoadenine (oxo-εA), which combines two adenine modifica-
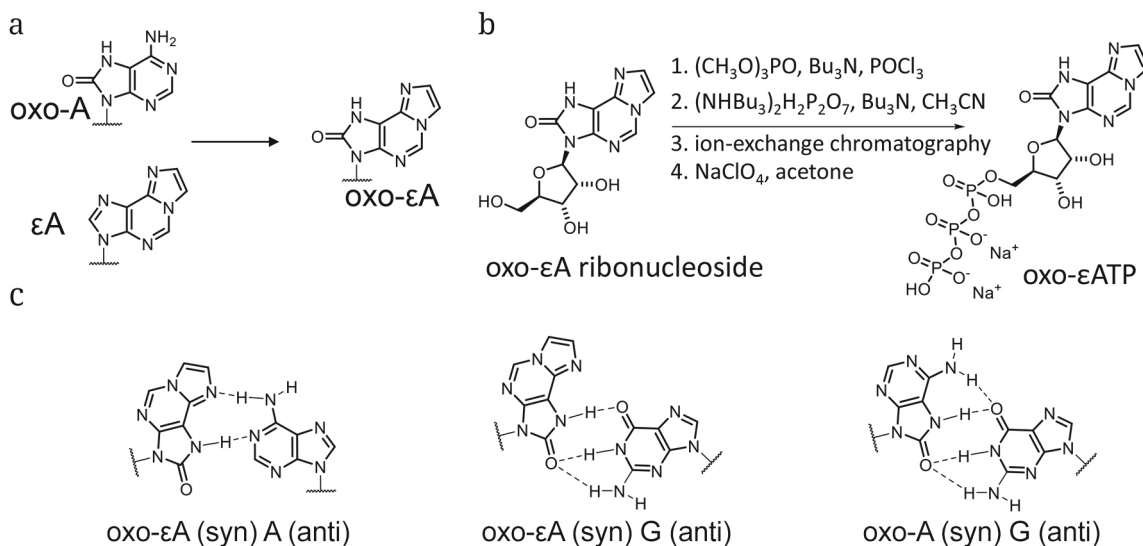
Fig. 1. Structure of oxo-εA (a), chemical synthesis of oxo-εATP (b), and geometry of oxo-εA:A, oxo-εA:G, and oxo-A:G pairs (c).

tions: 7,8-dihydro-8-oxoadenine (oxo-A) and 1,N^6-ethenoadenine (εA) (Fig. 1a). It was previously shown that DNA containing oxo-εA can be replicated by cellular DNA polymerases that incorporate A residues opposite oxo-εA [1]. The nitrogenous base of oxo-εA in the DNA duplex is predominantly in the *syn* conformation, forming a pair with adenine that is similar in its geometry to the AT pair [1]. This allows one to expect that oxo-εA triphosphate can potentially be incorporated into RNA.

The genome of SARS-CoV-2 is a single-stranded RNA molecule of 29.9 thousand nucleotides, which is replicated and transcribed by RdRp. This enzyme has a complex structure [2] and includes the catalytic subunit nsp12 and two auxiliary subunits (nsp7 and nsp8). The active site of RdRp is located in nsp12 and contains two aspartate residues, D760 and D761, involved in the binding of two divalent metal ions that play a key role in catalysis [3]. There is evidence that SARS-CoV-2 RdRp is one of the fastest viral polymerases (incorporation rate, 600 nt/s) [4], with a high error rate (up to 10^{-1}-10^{-3} misincorporations per nucleotide) [5]. Such a high error rate requires the presence of a proofreading activity, which is carried out by the 3′-5′ exoribonuclease nsp14 regulated by the viral protein nsp10 [6]. On the other hand, the high error rate contributes to the adaptation of viruses under selection conditions [7-9]. Despite a relatively low accuracy, RdRp is sensitive to the structure of nucleotide substrates. Thus, it strictly requires the presence of a 2′-OH group at the 3′-ends of both RNA primer and nucleotide substrate [10, 11]. At the same time, RdRp is capable of incorporating some phosphorylated synthetic nucleosides into the growing RNA strand, which has allowed the development of several nucleoside drugs (sofosbuvir [12, 13], remdesivir [14, 15],

and molnupiravir [16]). The incorporation of modified residues in the synthesized RNA can block its further elongation [13, 17, 18], while their presence in the RNA template can inhibit subsequent synthesis of the complementary RNA or increase the error rate [16, 19-21]. It was also shown that some natural modifications of the RNA template, such as N^1-methyladenosine, N^3-methyluridine, and 2′-O-methylguanosine, strongly block RNA extension by RdRp [11, 22].

Unlike most viral RNA-dependent RNA polymerases, bacterial, archaeal, and eukaryotic DNA-dependent RNA polymerases (RNAPs) are multisubunit proteins [23]. They also require Me^{2+} ions for catalysis [24, 25]. RNAPs have a lower error rate (10^{-3}-10^{-5}) in comparison with coronaviral RdRp [26, 27] but are also able to incorporate some modified nucleotide analogues [28-30]. Furthermore, RNAPs sense the presence of modified nucleotides in the DNA template. Depending on the nature of modification, RNAPs can incorporate an incorrect residue into the growing RNA chain opposite a lesion or can stop at the site of lesion, which makes them important sensors of DNA damage [31]. The presence of oxo-A in the template DNA strand is a serious obstacle for archaeal RNAP [32], while the presence of εA blocks the activity of bacterial RNAP [33]. However, it has been unknown how a combination of these two modifications can affect the activity of RNAP.

The purpose of this study was to analyze the effect of the oxo-εA modification in nucleotide substrates or in the template strand on the RNA synthesis by viral and prokaryotic RNA polymerases. We aimed to (i) establish whether RdRp is capable of incorporating 8-oxo-1,N^6-ethenoadenosine triphosphate (oxo-εATP) into the growing RNA opposite various template nucleotides, and whether the incorporation of the oxo-εA

residue inhibits further RNA synthesis and (ii) test whether *Escherichia coli* RNAP can use oxo-εATP as a substrate, as well as to investigate the effect of oxo-εA in the template DNA on the RNA synthesis by RNAP.

MATERIALS AND METHODS

Equipment and reagents for chemical synthesis. All reagents were purchased from Sigma-Aldrich (USA). Solvents were purchased from CHIMMED (Russia). ^{1}H, ^{13}C, and ^{31}P NMR spectra were recorded with a Bruker Avance III 600 spectrometer (Germany) at 600, 150, and 243 MHz, respectively. The multiplicity of signals in the spectra was indicated using the following abbreviations: s (singlet), d (doublet), and m (multiplet). The spin–spin coupling constants (J) are given in Hz. Ion-exchange chromatography was performed with an Akta Explorer 100 instrument (Cytiva, Sweden).

Synthesis and purification of the oxo-εATP disodium salt. Freshly distilled trimethyl phosphate [$(CH_3O)_3PO$] (8.0 mL) and tributylamine (Bu_3N) (0.95 mL) were added to oxo-εA ribonucleoside [34] (0.62 g, 2.0 mmol) in a Schlenk flask (100 mL) under inert gas atmosphere. The mixture was vigorously stirred at room temperature for 30 min and then cooled to −10°C. Phosphorus oxychloride ($POCl_3$) (0.33 mL, 3.6 mmol) was added under inert gas atmosphere and the mixture was stirred at −10°C for 1 h. Next, a phosphorylating mixture obtained by vigorously stirring acetonitrile CH_3CN (20 ml), Bu_3N (2.8 ml, 11.8 mmol) and bis(tributylammonium) pyrophosphate [$(NHBu_3)_2H_2P_2O_7$] (1.2 g, 2.2 mmol) under inert atmosphere for 20 min at −20°C, was added to the sample. After stirring the sample for 1 h at −10°C, cold water (65 ml) was added to the reaction mixture; the mixture was stirred for 1 h at 0°C, then transferred to a separatory funnel, and washed with methylene chloride (15 mL, 5 times). The aqueous layer was collected and aqueous ammonia solution was added to pH 7.0. The resulting oxo-εATP solution was stored in a refrigerator until purification by ion-exchange chromatography on a 50×250 mm column packed with HEMA-BIO 1000 DEAE 70 µm sorbent (Germany) with a gradient of 50-600 mM triethylammonium bicarbonate (pH 7.6). Fractions containing the target product were evaporated; the residue was re-dissolved in water and evaporated to remove residual buffer. The resulting product was converted to sodium salt by re-precipitation from aqueous solution with a tenfold volume of 3% sodium perchlorate ($NaClO_4$) solution in acetone. The precipitate was washed with dry acetone and dried under vacuum. The yield was 0.52 g (0.86 mmol, 43%). ^{1}H NMR (600 MHz, D_2O): δ 9.10 (s, 1H), 8.02 (d, J = 1.2 Hz, 1H), 7.63 (d, J = 1.2 Hz, 1H), 6.06 (d, J = 5.6 Hz, 1H), 5.36 (dd, J = 5.6 Hz, J = 5.7 Hz, 1H), 4.80-4.75 (m, 1H), 4.40-4.35 (m, 2H), 4.32-4.26 (m, 1H). ^{13}C NMR (150 MHz, D_2O): δ 154.1, 135.8, 135.4, 133.8, 132.9, 112.2, 108.4, 86.1, 82.9 (d, J = 8.4 Hz, 1C), 70.5, 69.9, 65.3 (d, J = 5.2 Hz, 1C). ^{31}P NMR (243 MHz, D_2O): δ −6.10 (d, J = 19.7 Hz, 1P), −10.79 (d, J = 18.8 Hz, 1P), −21.65 (dd, J = 19.7 Hz, J = 18.8 Hz, 1P) (see Online Resource 1 for NMR spectra).

Synthesis of DNA oligonucleotides with oxo-εA 2′-deoxyribonucleotide. Synthesis of oxo-εA 2′-deoxyribonucleotide 3′-phosphoramidite and modified DNA oligonucleotides was performed as described previously [1]. Briefly, modified DNA oligonucleotides were prepared using the solid-phase phosphoramidite method in a MerMade 12 synthesizer (Bioautomation, USA). Protected 2′-deoxyribonucleoside 3′-phosphoramidites, Unylinker-CPG (500 Å), and S-ethylthio-1H-tetrazole were purchased from ChemGenes (USA). The synthesis used a standard deprotection protocol by treatment with aqueous saturated ammonia at 55°C overnight. The solutions were evaporated, and the aliquots were analyzed by HPLC (purity, >95%). Analysis and purification of oligonucleotides by HPLC was performed on a 4.6×250 mm Jupiter C18 column (5 µm, Phenomenex, USA) with an Agilent 1260 HPLC system (USA) equipped with an autosampler and a fraction collector. Buffer A: 0.05 M ammonium acetate (pH 7.0), 5% acetonitrile; buffer B: 0.03 M ammonium acetate, 80% acetonitrile (pH 7.0); gradient B: 0→15% (1 column volume), 15→50% (10 column volumes); flow rate 1 ml/min; temperature 45°C.

Protein expression and purification. SARS-CoV-2 RdRp was obtained by heterologous expression in *E. coli* BL-21(DE3) cells and purified by Ni-affinity and anion-exchange chromatographies as described previously [11]. *E. coli* RNAP core enzyme was expressed in the same strain using the pVS10 vector and purified by polyethyleneimine precipitation followed by heparin, Ni-affinity, and anion-exchange chromatography as described previously [35].

***In vitro* RNA synthesis by SARS-CoV-2 RdRp.** The ability of RdRp to incorporate oxo-εATP was analyzed using RNA oligonucleotides (DNA Synthesis, Russia) corresponding to the RNA primer and RNA template. The radioactive label was introduced at the 5′-end of the primer by T4 polynucleotide kinase (New England Biolabs, USA) using 0.8 MBq γ-[^{32}P]ATP (Shemyakin–Ovchinnikov Institute of Bioorganic Chemistry) according to the manufacturer's protocol. The RNA substrate was obtained by mixing the labeled primer and the template to the final concentrations of 2 µM and 2.2 µM, respectively, in the transcription buffer (TB) containing 10 mM Tris-HCl, pH 7.9, 10 mM KCl, and 0.1 mM EDTA (all reagents from Sigma-Aldrich unless indicated otherwise). The mixture was heated at 95°C for 3 min, then cooled to 85°C in 2 min,

and gradually cooled to 25°C at 0.5°C/min. The RNA substrate was diluted with TB and mixed with RdRp to the final concentrations of 25 nM and 500 nM, respectively, and the mixture was incubated at 30°C for 10 min. The reaction was started by adding a mixture of NTPs (Illustra, UK) and $MgCl_2$ or $MnCl_2$ (Sigma-Aldrich) to the final concentrations of 10 µM and 1.1 mM, respectively. Oxo-εATP was added to 100 µM when indicated. Transcription was performed at 30°C for various time intervals (from 30 s to 10 min). The reaction was stopped by adding an equal volume of stop solution containing formamide (Vekton, Russia) and heparin (100 µg/ml, Sigma-Aldrich), and the samples were heated at 95°C for 3 min. RNA products were separated by 15% PAGE (19 : 1) under denaturing conditions (7.5 M urea, Roth, Germany) in TBE buffer and detected using a Typhoon 9500 scanner (GE Healthcare, USA).

***In vitro* transcription with *E. coli* RNAP.** The ability of RNAP to incorporate oxo-εATP into RNA and to pass oxo-εA in the template DNA strand was analyzed using RNA and DNA oligonucleotides corresponding to the RNA transcript and DNA template and nontemplate strands. Unmodified oligonucleotides were synthesized by Sintol (Russia). A 5′-terminal radioactive label was introduced into RNA as described above. Labeled RNA oligonucleotide was mixed with the template DNA strand to the final concentrations of 1 and 2 µM, respectively, in transcription buffer 2 (TB2) containing 40 mM Tris-HCl, pH 7.9, 40 mM KCl, and 0.1 mM EDTA. The mixture was heated at 65°C for 3 min, and then gradually cooled to 25°C at 0.5°C/min. The annealed duplex was diluted with TB2 to 250 nM and *E. coli* RNAP core enzyme was added to 1 µM (in experiments with oxo-εATP) or to 2 µM (in experiments with oxo-εdA DNA templates). The samples were incubated at 37°C for 10 min. The nontemplate strand was added to the final concentration of 2.5 µM and the samples were incubated at 37°C for 15 min. The reconstituted elongation complex was diluted 10-fold with TB2. The reaction was started by adding a mixture of NTPs (Illustra, UK) and $MgCl_2$ or $MnCl_2$ (Sigma-Aldrich) to the final concentrations of 10 µM and 10 mM, respectively. Oxo-εATP was added to 100 µM when indicated. Transcription was performed at 37°C for 30 s. The reaction was stopped by adding an equal volume of stop buffer containing 8 M urea (Roth, Germany), 30 mM EDTA (Sigma-Aldrich), and 2× TBE. Transcription products were separated by PAGE as described above.

RESULTS

Chemical synthesis of oxo-εATP. Oxo-εATP was prepared starting from 7,8-dihydro-8-oxo-1,*N6*-ethe-noadenosine (oxo-εA ribonucleoside) [34] and following the procedure described in [36] with minor modifications (Fig. 1b). Briefly, oxo-εA ribonucleoside was treated with $POCl_3$ in the presence of Bu_3N in $(CH_3O)_3PO$ as a solvent to produce the corresponding nucleoside dichlorophosphoridate, whose reaction with $(NHBu_3)_2H_2P_2O_7$ and subsequent hydrolysis of the resulting cyclic intermediate produced crude oxo-εATP, which was purified by ion exchange chromatography and precipitated with $NaClO_4$ in acetone to obtain the required product (yield, 43%).

Incorporation of oxo-εATP by RdRp into nascent RNA. First, we tested the ability of SARS-CoV-2 RdRp to incorporate the triphosphorylated form of oxo-εA (oxo-εATP) into the growing RNA chain. For this purpose, we used a model system (Fig. 2a) that had been previously used in the studies of the biochemical activity of RdRp and its inhibitors [11, 37-39]. The RdRp enzyme used in the reactions contained the catalytic subunit nsp12 and the accessory subunits nsp7 and nsp8 fused to each other. The RNA substrate consisted of two complementary RNA oligonucleotides, an RNA primer containing a radioactive label at the 5′-end, and an RNA template strand. RdRp was first incubated with the RNA substrate to form a complex, then nucleotides were added, and the reaction was carried out for 10 min at 30°C. When RdRp and a full set of unmodified NTPs were added, effective elongation of the original primer occurred in the presence of either Mg^{2+} and Mn^{2+} ions (Fig. 2b, lanes 9 and 18). By adding various sets of NTPs, we determined the efficiency of oxo-εA incorporation opposite different template bases. The G residue was located at the +1 position of the template (Fig. 2a). The addition of oxo-εATP in the presence of Mg^{2+} ions does not lead to the elongation of the RNA primer (lane 2, compare with the control sample in lane 1). In the control experiment with CTP (lane 3), most of the primer was elongated by 1-2 nucleotides (probably due to the incorporation of CTP opposite the first G and second A residues, which is consistent with the published data on a relatively low accuracy of SARS-CoV-2 RdRp [5]). In the presence of Mn^{2+} ions, RdRp acquired the ability to incorporate two oxo-εA residues opposite G and A in the RNA template (lane 11, compare with the control sample in lane 20), and also incorporated two C residues opposite G and A (lane 12).

When CTP and oxo-εATP were added together in the presence of either Mg^{2+} and Mn^{2+} ions, they were sequentially incorporated, as evidenced by a slower electrophoretic mobility of the 37-nt RNA product (lanes 4 and 13) compared to the reactions performed with CTP only (lanes 3 and 12). Therefore, under these conditions, oxo-εA was incorporated opposite the template residue A with a greater efficiency than CTP (which was also present in reactions in lanes 4 and 13).
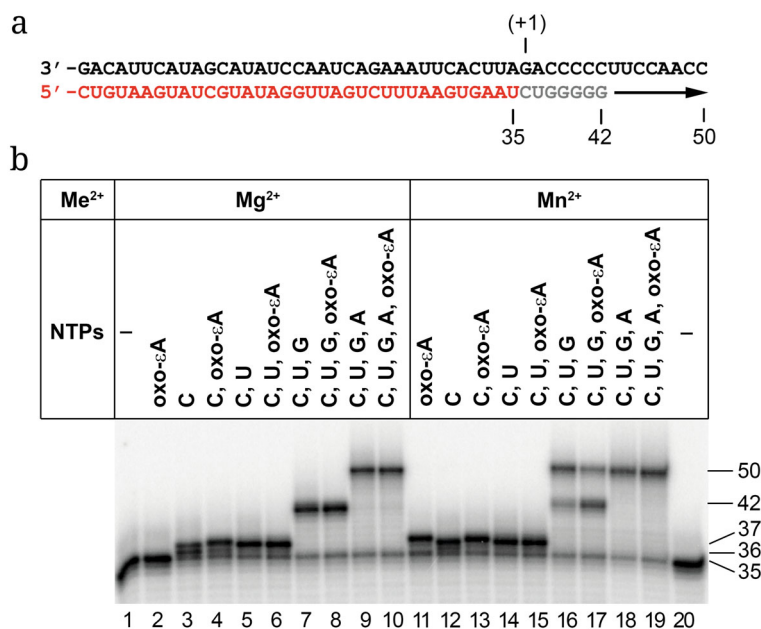
Fig. 2. Incorporation of oxo-εATP by SARS-CoV-2 RdRp. a) RNA substrate used in the experiments. Red, RNA primer; black, RNA template; the first template base is marked +1; gray, residues incorporated by RdRp upon primer extension (7 residues incorporated upon addition of CTP, UTP, and GTP); arrow, direction of transcription. b) Analysis of RNA extension products synthesized in the presence of different sets of NTPs and oxo-εATP with Mg^{2+} (left panel) and Mn^{2+} (right panel). The length of RNA products (nt) is indicated on the right. The products were separated by 15% denaturing PAGE.

When CTP and UTP were added, RNA was elongated by 2 nucleotides with the formation of the expected 37-nt product (lanes 7 and 14). When a mixture of CTP, UTP, and oxo-εATP was added, no further elongation of the 37-nt product was observed (lanes 6 and 15). Hence, oxo-εAp was not incorporated by RdRp opposite the template C in the next position. Addition of CTP, UTP, and GTP in the presence of Mg^{2+} led to the formation of a stalled complex with a 42-nt RNA transcript (lane 7), which was not elongated when oxo-εATP was added to the reaction (lane 8). Therefore, RdRp did not incorporate oxo-εATP opposite the template U in the next position. Interestingly, in the presence of Mn^{2+}, a significant portion of the elongation complexes extended RNA beyond 42 nt, apparently, by including non-complementary NTPs (lane 16); the presence of oxo-εATP partially inhibited this reaction (lane 17). When all 4 NTPs were added, no difference in the electrophoretic mobility of RNA products was observed in the presence or absence of oxo-εATP with either Mg^{2+} (lanes 9 and 10) or Mn^{2+} (lanes 18 and 19). Hence, no significant oxo-εATP incorporation was observed in the presence of natural NTPs, and oxo-εATP did not inhibit the activity of RdRp.

For a more detailed analysis of oxo-εATP incorporation by RdRp, we modified the test system. To test oxo-εATP incorporation opposite each of the template nucleotides under the same conditions, 4 identical RNA templates with different template nucleotides at the +1 position were synthesized. In addition, a shorter RNA primer was used for better separation of RNA products by PAGE (Fig. 3a). In order to reduce the incorporation of incorrect (not forming a canonical Watson–Crick pair) nucleotides, the reaction time was reduced to 30 s. It was shown that in the presence of Mg^{2+} ions, RdRp with a high efficiency incorporated NTPs that formed canonical base pairs (UTP, GTP, GTP, and ATP in the case of template A, G, C, and U residues, respectively; Fig. 3b, lanes 2, 6, 8, and 10), but almost did not incorporate oxo-εATP (lanes 3, 7, 9, and 11).

A different pattern of nucleotide incorporation was observed in the presence of Mn^{2+} ions. In this case, in the control reactions, each of the nucleotides was incorporated not only opposite the corresponding template residue, but also in the next position, opposite the template U (Fig. 3c, lanes 2, 7, 10, and 12). In the reactions with oxo-εATP, the modified nucleotide was incorporated with a high efficiency opposite the template residues A and G (Fig. 3c, lanes 3 and 7), but not opposite C and U (lanes 11 and 13). In the case of the A and G templates in the presence of oxo-εATP and ATP, the RNA primer was further elongated (by a total of 4 nt), which demonstrated the ability of RdRp to incorporate both oxo-εATP and ATP into the synthesized RNA.

Incorporation of oxo-εATP by RNAP into nascent RNA. To understand whether the observed ability of RdRp to incorporate oxo-εATP is a universal phenomenon, we tested if cellular DNA-dependent RNA polymerase from *E. coli*, which is unrelated to RdRp,
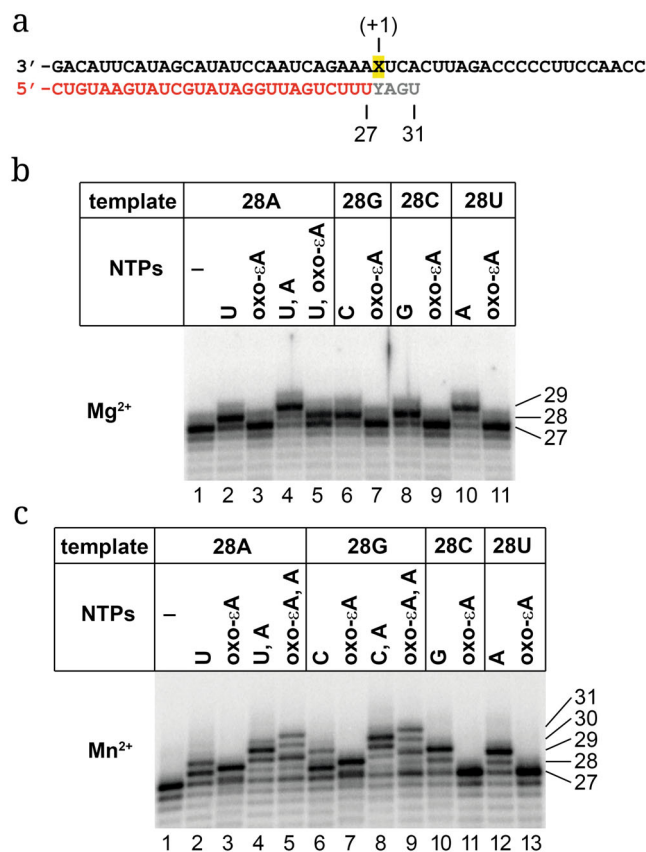
Fig. 3. Incorporation of oxo-εATP by RdRp using RNA substrates with different template bases at the +1 position. a) RNA substrates used in the experiments. Red, RNA primer; black, RNA template; yellow, variable template base at +1 position (X); gray, residue incorporated opposite it (Y) and the next three residues. b and c) Analysis of RNA extension products obtained in the presence of natural NTPs and/or oxo-εATP with Mg^{2+} (b) and Mn^{2+} (c) ions. The reactions were carried out with RNA templates containing A, G, C, or U at the +1 position. RNA products were separated by 15% denaturing PAGE. The length of the RNA products (nt) is shown on the right.

can perform similar reactions. Unlike RdRp, RNAP synthesizes RNA by moving along a double-stranded DNA and melting the DNA strands during RNA elongation. In this case, a synthetic elongation complex containing the core enzyme of *E. coli* RNAP, a short RNA transcript (20 nt), and DNA template and nontemplate strands was prepared from oligonucleotides as described previously (Fig. 4a) [40-42]. As can be seen in Fig. 4b, oxo-εATP was not incorporated opposite dG at position +1 in the template strand in the presence of either Mg^{2+} or Mn^{2+} (lanes 2 and 12). Addition of CTP or CTP and GTP resulted in RNA elongation by 1 or 3 nucleotides (to 21 or 23 nt), but these RNA products were not extended further upon addition of oxo-εATP (lanes 3-6 and 13-16). Therefore, oxo-εATP also cannot be incorporated opposite dC and dT residues in the next template positions. Addition of CTP, GTP, and ATP resulted in transcription stalling after addition of 4 nucleotides, in accordance with the template sequence (24-nt RNAs were synthesized; lanes 7 and 17). In the presence of oxo-εATP, additional RNA elongation by two more nucleotides (to 26 nt) was

observed, which was more efficient in the presence of Mn^{2+} ions (lanes 8 and 18). Probably, this involved incorporation of oxo-εA at position 25 of RNA opposite the template dA and further RNA extension due to the incorporation of G opposite the template dC at position 26. However, since transcription stopped after this, oxo-εATP is not a functional analogue of UTP. Finally, when oxo-εATP and the full set of NTPs were added together, no difference in the RNA products was observed with the control reaction without oxo-εATP (lanes 9, 10, 19, and 20).

Incorporation of NTPs opposite oxo-εA by RNAP. Finally, we studied the effects of oxo-εA residue in the template DNA strand on RNA synthesis by RNAP. For this purpose, synthetic elongation complexes were assembled as described above using template DNA oligonucleotides containing a deoxyribonucleotide derivative of oxo-εA or control unmodified dA at +2 position relative to the 3′-end of the RNA primer (+1 template nucleotide in these templates was also dA; Fig. 5a). It was found that with the control template, RNAP added complementary NTPs
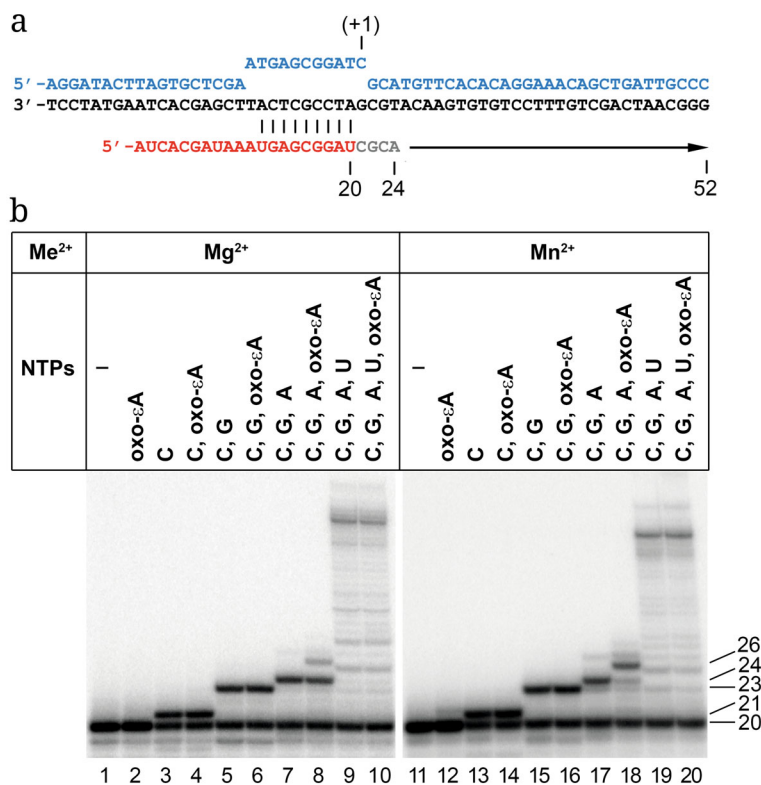
a

b

Fig. 4. Incorporation of oxo-εATP by *E. coli* RNAP. a) Elongation complex used in the experiments. Red, RNA oligonucleotide; black, template DNA strand; blue, non-template strand; gray, the first 4 incorporated nucleotide residues; arrow, direction of transcription; the starting point of nucleotide incorporation (+1) is shown. b) Analysis of transcription products synthesized in the presence of various sets of NTPs and oxo-εATP with Mg^{2+} (left panel) and Mn^{2+} (right panel) ions. RNA products were separated by 15% denaturing PAGE. The length of RNA products (nt) is indicated on the right.

to the growing RNA chain as expected: UTP (17-nt RNA was extended by 2 nt to 19 nt; Fig. 5b, lane 10), UTP and GTP (RNA was extended by 4 nt to 21 nt; lane 12), or all four NTPs (lane 16). In agreement with the previous experiments, weak incorporation of oxo-εATP opposite the template dA was also observed (lane 15). When the elongation complex contained oxo-εA at +2 position of the template strand, only the first UTP residue was incorporated opposite the template dA residues at +1 position in all reactions, after which the synthesis stopped and further NTP incorporation opposite template oxo-εA did not occur (Fig. 5c, lanes 2-8).

DISCUSSION

We found that synthetic ATP analogue oxo-εATP can be incorporated into the nascent RNA by two unrelated RNA polymerases. This suggests that oxo-εATP can be accommodated in the active site of the enzymes due to its small size and similarity to natural nucleotides. Furthermore, since Watson-Crick interactions are blocked by the etheno modification, oxo-εATP probably adopts the *syn* conformation and pairs with the purine base of the template nucleotide

at the +1 position, forming a pair similar to oxo-εA:A [1] or oxo-A:G [43] in the DNA context (Fig. 1c). This explains the observed preference for oxo-εATP incorporation opposite purine nucleotides of the template. In the presence of Mg^{2+} ions, SARS-CoV-2 RdRp slowly incorporated oxo-εATP opposite the template A (compare the incorporation efficiencies at 10 min in Fig. 2, lane 4, and at 30 s in Fig. 3, lane 3). The situation changed in the presence of Mn^{2+} ions, when incorporation was observed opposite both A and G. In the case of *E. coli* RNAP, oxo-εATP was incorporated only opposite dA, but the efficiency of such incorporation also increased in the presence of Mn^{2+} ions. This difference is probably due to the structural features of the active site of cellular RNAPs, which ensures a greater accuracy of RNA synthesis, since the oxo-εA:dA pair is more similar to the canonical one than the oxo-εA:dG pair (Fig. 1c). The stimulatory effect of manganese ions on the oxo-εATP incorporation observed for both RNA polymerases is likely due to the difference in the chemical properties and sizes of Mn^{2+} and Mg^{2+} cations. Previously, analysis of RNA synthesis by poliovirus RdRp demonstrated that the fidelity of NTP incorporation in the presence of Mg^{2+} is controlled at two steps: reorientation of the triphosphate
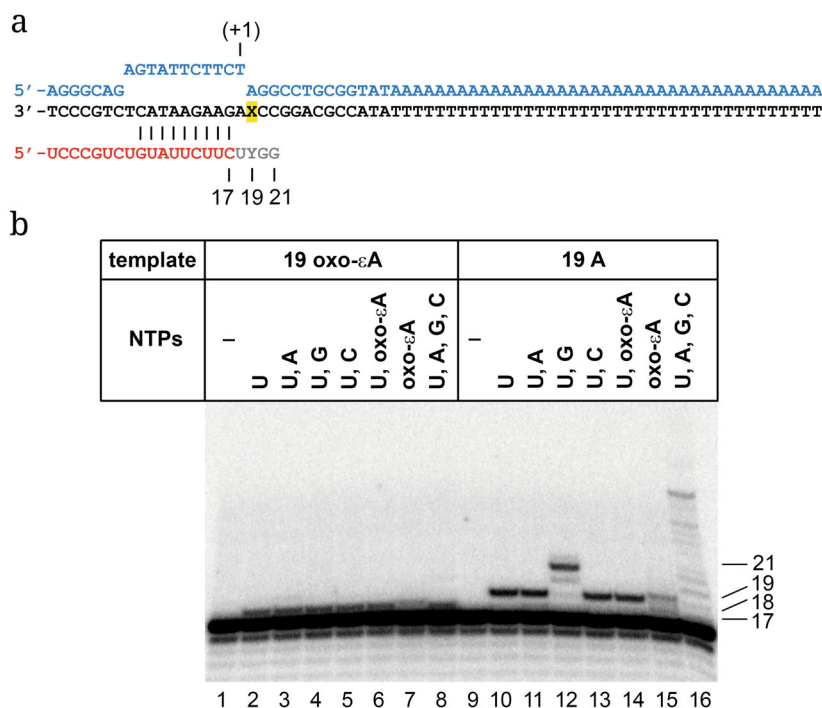
Fig. 5. Incorporation of nucleotides against oxo-εA in the template DNA strand by *E. coli* RNAP. a) Elongation complex used in the experiments. Red, RNA oligonucleotide; black, template strand; blue, non-template strand is blue; yellow, position of oxo-εdA or control dA (X); Y, residue incorporated opposite oxo-εA or dA; gray, the first 4 incorporated nucleotide residues; starting point of nucleotide incorporation (+1) is shown. b) Analysis of transcription products synthesized by RNAP on the oxo-εA (left panel) or control dA (right panel) templates. RNA products were separated by 15% denaturing PAGE. The length of the RNA products (nt) is indicated on the right.

of the incoming NTP and phosphoryl transfer [44]. In the presence of Mn^{2+}, RdRp loses its ability to use the phosphoryl transfer step to control the fidelity because of the same incorporation rate for complementary and non-complementary NTPs [45], which results in a decreased fidelity of RdRp in the presence of Mn^{2+} [46-48]. The observed differences during incorporation of non-complementary and unnatural NTPs may be due to the differences in the sizes of these cations. Mn^{2+} ion has a smaller radius than Mg^{2+}, which frees up space in the active site and allows the non-canonical pair to be oriented in a position favorable for catalysis. It was also shown for that the reactions of exo- and endonucleolytic cleavage by RNA *E. coli* RNAP, which are carried out in the same active site of the enzyme as RNA synthesis, proceed faster in the presence of Mn^{2+} ions [25, 49]. This indicates the ability of Mn^{2+} to change the nucleophilic properties of reacting molecules (in this case, water) [49]. There is also evidence that the binding of Mn^{2+} ion increases the flexibility of RdRp molecule [50], which can additionally facilitate incorporation of NTPs forming noncanonical base pairs. Further research is needed for better understanding of the observed phenomenon. At the same time, the replacement of standard Mg^{2+} cation with Mn^{2+} can be used for enzymatic incorporation of modified NTPs into synthesized RNA for practical purposes.

Since it was previously shown that oxo-εA can be bypassed by DNA polymerases *in vivo* [1], it could be expected that cellular RNAP would also be able to incorporate nucleotides opposite the template oxo-εA. However, it was found that the presence of oxo-εA in the template strand completely blocked the RNAP activity even with Mn^{2+} ions. The observed difference (oxo-εATP can be incorporated into RNA, but stalls RNA extension when present in the DNA template) is also probably due to the structure of the RNAP active site. After translocation, the nucleotide residue at +1 position of the template DNA strand is fixed in the active site [51], while the incoming NTP can be bound in different configurations [51], i.e., it is more flexible than the template base, which may allow it to occupy a position more favorable for catalysis.

Although the studied RNA polymerases are able to incorporate oxo-εATP into the synthesized RNA, we failed to observe the inhibitory activity of oxo-εATP on the incorporation of unmodified nucleotides. Despite a 10-fold excess of oxo-εATP over natural NTPs, the studied RNA polymerases did not incorporate it in the presence of a full set of NTPs, and oxo-εATP did not suppress incorporation of complementary nucleotides. Therefore, oxo-εA is not a potential antiviral or antibacterial transcription inhibitor; however, it may be a prototype for obtaining more effective transcription

inhibitors by further modifications. Considering its fluorescent properties [1], oxo-εA can also be used as a label in studying the mechanisms of RdRp interaction with RNA and nucleotide substrates. Based on our data, it can be proposed that the simultaneous modification of the Watson–Crick and Hoogsteen edges of purine bases leading to the redistribution of potential hydrogen bonds and favoring the *syn* conformation makes such modified nucleotides weak inhibitors of viral and bacterial RNAPs.

Contributions. A.V.A., A.V.K., and I.V.P. planned the study; A.V.A, I.A.I., M.S.B., and T.S.Z. synthesized and purified oxo-εATP and modified DNA oligonucleotides, I.V.P performed the experiments; A.V.A., A.V.K., and I.V.P. discussed the results and wrote the article.

Ethics declarations. This work does not contain any studies involving human or animal subjects. The authors of this work declare that they have no conflicts of interest.

REFERENCES

1. Aralov, A. V., Gubina, N., Cabrero, C., Tsvetkov, V. B., Turaev, A. V., Fedeles, B. I., Croy, R. G., Isaakova, E. A., Melnik, D., Dukova, S., Ryazantsev, D. Y., Khrulev, A. A., Varizhuk, A. M., Gonzalez, C., Zatsepin, T. S., and Essigmann, J. M. (2022) 7,8-Dihydro-8-oxo-1,N6-ethenoadenine: an exclusively Hoogsteen-paired thymine mimic in DNA that induces A→T transversions in *Escherichia coli*, *Nucleic Acids Res.*, **50**, 3056-3069, https://doi.org/10.1093/nar/gkac148.

2. Kim, D., Lee, J.-Y., Yang, J.-S., Kim, J. W., Kim, V. N., and Chang, H. (2020) The architecture of SARS-CoV-2 transcriptome, *Cell*, **181**, 914-921.e910, https://doi.org/10.1016/j.cell.2020.04.011.

3. Hillen, H. S., Kokic, G., Farnung, L., Dienemann, C., Tegunov, D., and Cramer, P. (2020) Structure of replicating SARS-CoV-2 polymerase, *Nature*, **584**, 154-156, https://doi.org/10.1038/s41586-020-2368-8.

4. Shannon, A., Selisko, B., Le, N. T., Huchting, J., Touret, F., Piorkowski, G., Fattorini, V., Ferron, F., Decroly, E., Meier, C., Coutard, B., Peersen, O., and Canard, B. (2020) Rapid incorporation of Favipiravir by the fast and permissive viral RNA polymerase complex results in SARS-CoV-2 lethal mutagenesis, *Nat. Commun.*, **11**, 4682, https://doi.org/10.1038/s41467-020-18463-z.

5. Yin, X., Popa, H., Stapon, A., Bouda, E., and Garcia-Diaz, M. (2023) Fidelity of ribonucleotide incorporation by the SARS-CoV-2 replication complex, *J. Mol. Biol.*, **435**, 167973, https://doi.org/10.1016/j.jmb.2023.167973.

6. Moeller, N. H., Shi, K., Demir, O., Belica, C., Banerjee, S., Yin, L., Durfee, C., Amaro, R. E., and Aihara, H. (2022) Structure and dynamics of SARS-CoV-2 proofreading exoribonuclease ExoN, *Proc. Natl. Acad. Sci. USA*, **119**, e2106379119, https://doi.org/10.1073/pnas.2106379119.

7. Drake, J. W., and Holland, J. J. (1999) Mutation rates among RNA viruses, *Proc. Natl. Acad. Sci. USA*, **96**, 13910-13913, https://doi.org/10.1073/pnas.96.24.13910.

8. Jenkins, G. M., Rambaut, A., Pybus, O. G., and Holmes, E. C. (2002) Rates of molecular evolution in RNA viruses: a quantitative phylogenetic analysis, *J. Mol. Evol.*, **54**, 156-165, https://doi.org/10.1007/s00239-001-0064-3.

9. Sanjuan, R., Nebot, M. R., Chirico, N., Mansky, L. M., and Belshaw, R. (2010) Viral mutation rates, *J. Virol.*, **84**, 9733-9748, https://doi.org/10.1128/JVI.00694-10.

10. Jones, A. N., Mourao, A., Czarna, A., Matsuda, A., Fino, R., Pyrc, K., Sattler, M., and Popowicz, G. M. (2022) Characterization of SARS-CoV-2 replication complex elongation and proofreading activity, *Sci. Rep.*, **12**, 9593, https://doi.org/10.1038/s41598-022-13380-1.

11. Petushkov, I., Esyunina, D., and Kulbachinskiy, A. (2023) Effects of natural RNA modifications on the activity of SARS-CoV-2 RNA-dependent RNA polymerase, *FEBS J.*, **290**, 80-92, https://doi.org/10.1111/febs.16587.

12. Sacramento, C. Q., Fintelman-Rodrigues, N., Temerozo, J. R., Da Silva, A. P. D., Dias, S., da Silva, C. D. S., Ferreira, A. C., Mattos, M., Pao, C. R. R., de Freitas, C. S., Soares, V. C., Hoelz, L. V. B., Fernandes, T. V. A., Branco, F. S. C., Bastos, M. M., Boechat, N., Saraiva, F. B.,

Ferreira, M. A., Jockusch, S., Wang, X., et al. (2021) In vitro antiviral activity of the anti-HCV drugs daclatasvir and sofosbuvir against SARS-CoV-2, the aetiological agent of COVID-19, *J. Antimicrob. Chemother.*, **76**, 1874-1885, https://doi.org/10.1093/jac/dkab072.

13. Jockusch, S., Tao, C., Li, X., Chien, M., Kumar, S., Morozova, I., Kalachikov, S., Russo, J. J., and Ju, J. (2020) Sofosbuvir terminated RNA is more resistant to SARS-CoV-2 proofreader than RNA terminated by Remdesivir, *Sci. Rep.*, **10**, 16577, https://doi.org/10.1038/s41598-020-73641-9.

14. Kokic, G., Hillen, H. S., Tegunov, D., Dienemann, C., Seitz, F., Schmitzova, J., Farnung, L., Siewert, A., Hobartner, C., and Cramer, P. (2021) Mechanism of SARS-CoV-2 polymerase stalling by remdesivir, *Nat. Commun.*, **12**, 279, https://doi.org/10.1038/s41467-020-20542-0.

15. Yin, W. M. C., Luan, X., Shen, D. D., Shen, Q., Su, H., Wang, X., Zhou, F., Zhao, W., Gao, M., Chang, S., Xie, Y. C., Tian, G., Jiang, H. W., Tao, S. C., Shen, J., Jiang, Y., Jiang, H., Xu, Y., Zhang, S., Zhang, Y., and Xu, H. E. (2020) Structural basis for inhibition of the RNA-dependentRNA polymerase from SARS-CoV-2 by remdesivir, *Science*, **368**, 1499-1504, https://doi.org/10.1126/science.abc1560.

16. Kabinger, F. S. C., Schmitzová, J., Dienemann, C., Kokic, G., Hillen, H. S., Höbartner, C., and Cramer, P. (2021) Mechanism of molnupiravir-induced SARS-CoV-2 mutagenesis, *Nat. Struct. Mol. Biol.*, **28**, 740-746, https://doi.org/10.1038/s41594-021-00651-0.

17. Wang, J., Shi, Y., Reiss, K., Maschietto, F., Lolis, E., Konigsberg, W. H., Lisi, G. P., and Batista, V. S. (2022) Structural insights into binding of remdesivir triphosphate within the replication–transcription complex of SARS-CoV-2, *Biochemistry*, **61**, 1966-1973, https://doi.org/10.1021/acs.biochem.2c00341.

18. Gordon, C. J., Tchesnokov, E. P., Woolner, E., Perry, J. K., Feng, J. Y., Porter, D. P., and Götte, M. (2020) Remdesivir is a direct-acting antiviral that inhibits RNA-dependent RNA polymerase from severe acute respiratory syndrome coronavirus 2 with high potency, *J. Biol. Chem.*, **295**, 6785-6797, https://doi.org/10.1074/jbc.RA120.013679.

19. Gordon, C. J., Tchesnokov, E. P., Schinazi, R. F., and Götte, M. (2021) Molnupiravir promotes SARS-CoV-2 mutagenesis via the RNA template, *J. Biol. Chem.*, **297**, 100770, https://doi.org/10.1016/j.jbc.2021.100770.

20. Tchesnokov, E. P., Gordon, C. J., Woolner, E., Kocinkova, D., Perry, J. K., Feng, J. Y., Porter, D. P., and Götte, M. (2020) Template-dependent inhibition of coronavirus RNA-dependent RNA polymerase by remdesivir reveals a second mechanism of action, *J. Biol. Chem.*, **295**, 16156-16165, https://doi.org/10.1074/jbc.AC120.015720.

21. Luo, X., Wang, X., Yao, Y., Gao, X., and Zhang, L. (2022) Unveiling the "template-dependent" inhibition on the viral transcription of SARS-CoV-2, *J. Phys. Chem. Lett.*, **13**, 7197-7205, https://doi.org/10.1021/acs.jpclett.2c01314.

22. Apostle, A., Yin, Y., Chillar, K., Eriyagama, A., Arneson, R., Burke, E., Fang, S., and Yuan, Y. (2023) Effects of epitranscriptomic RNA modifications on the catalytic activity of the SARS-CoV-2 replication complex, *Chembiochem*, **24**, e202300095, https://doi.org/10.1002/cbic.202300095.

23. Iyer, L. M., and Aravind, L. (2012) Insights from the architecture of the bacterial transcription apparatus, *J. Struct. Biol.*, **179**, 299-319, https://doi.org/10.1016/j.jsb.2011.12.013.

24. Steitz, T. A. (1998) A mechanism for all polymerases, *Nature*, **391**, 231-232, https://doi.org/10.1038/34542.

25. Sosunov, V., Sosunova, E., Mustaev, A., Bass, I., Nikiforov, V., and Goldfarb, A. (2003) Unified two-metal mechanism of RNA synthesis and degradation by RNA polymerase, *EMBO J.*, **22**, 2234-2244, https://doi.org/10.1093/emboj/cdg193.

26. James, K., Gamba, P., Cockell, S. J., and Zenkin, N. (2017) Misincorporation by RNA polymerase is a major source of transcription pausing *in vivo*, *Nucleic Acids Res.*, **45**, 1105-1113, https://doi.org/10.1093/nar/gkw969.

27. Imashimizu, M., Oshima, T., Lubkowska, L., and Kashlev, M. (2013) Direct assessment of transcription fidelity by high-resolution RNA sequencing, *Nucleic Acids Res.*, **41**, 9090-9104, https://doi.org/10.1093/nar/gkt698.

28. Mäkinen, J., Shin, Y., Vieras, E., Virta, P., Metsä-Ketelä, M., Murakami, K., and Belogurov, G. (2021) The mechanism of the nucleo-sugar selection by multi-subunit RNA polymerases, *Nat. Commun.*, **12**, 796, https://doi.org/10.1038/s41467-021-21005-w.

29. Nedialkov, Y. A., and Burton, Z. F. (2013) Translocation and fidelity of *Escherichia coli* RNA polymerase, *Transcription*, **4**, 136-143, https://doi.org/10.4161/trns.25527.

30. Nudler, E., Gusarov, I., and Bar-Nahum, G. (2003) Methods of Walking with the RNA Polymerase, in *Methods in Enzymology*, Academic Press, pp. 160-169, https://doi.org/10.1016/S0076-6879(03)71011-8.

31. Agapov, A., Olina, A., and Kulbachinskiy, A. (2022) RNA polymerase pausing, stalling and bypass during transcription of damaged DNA: from molecular basis to functional consequences, *Nucleic Acids Res.*, **50**, 3018-3041, https://doi.org/10.1093/nar/gkac174.

32. Gehring, A. M., and Santangelo, T. J. (2017) Archaeal RNA polymerase arrests transcription at DNA lesions, *Transcription*, **8**, 288-296, https://doi.org/10.1080/21541264.2017.1324941.

33. Pupov, D., Ignatov, A., Agapov, A., and Kulbachinskiy, A. (2019) Distinct effects of DNA lesions on RNA synthesis by *Escherichia coli* RNA polymerase, *Biochem. Biophys.*

Res. Commun., **510**, 122-127, https://doi.org/10.1016/j.bbrc.2019.01.062.

34. Guseva, E. A., Kamzeeva, P. N., Sokolskaya, S. Y., Slushko, G. K., Belyaev, E. S., Myasnikov, B. P., Golubeva, J. A., Alferova, V. A., Sergiev, P. V., and Aralov, A. V. (2024) Modified (2′-deoxy)adenosines activate autophagy primarily through AMPK/ULK1-dependent pathway, *Bioorg. Med. Chem. Lett.*, **113**, 129980, https://doi.org/10.1016/j.bmcl.2024.129980.

35. Svetlov, V., and Artsimovitch, I. (2015) Purification of bacterial RNA polymerase: tools and protocols, *Methods Mol. Biol.*, **1276**, 13-29, https://doi.org/10.1007/978-1-4939-2392-2_2.

36. Kore, A. R., Shanmugasundaram, M., Senthilvelan, A., and Srinivasan, B. (2012) Gram-scale chemical synthesis of 2′-deoxynucleoside-5′-O-triphosphates, *Curr. Protocols Nucleic Acid Chem.*, **49**, 13.10.11-13.10.12, https://doi.org/10.1002/0471142700.nc1310s49.

37. Kamzeeva, P., Petushkov, I., Knizhnik, E., Snoeck, R., Khodarovich, Y., Ryabukhina, E., Alferova, V., Eshtukov-Shcheglov, A., Belyaev, E., Svetlova, J., Vedekhina, T., Kulbachinskiy, A., Varizhuk, A., Andrei, G., and Aralov, A. (2023) Phenotypic test of benzo[4,5]imidazo[1,2-c]pyrimidinone-based nucleoside and non-nucleoside derivatives against DNA and RNA viruses, including coronaviruses, *Int. J. Mol. Sci.,* **24**, 14540, https://doi.org/10.3390/ijms241914540.

38. Miropolskaya, N., Kozlov, M., Petushkov, I., Prostova, M., Pupov, D., Esyunina, D., Kochetkov, S., and Kulbachinskiy, A. (2023) Effects of natural polymorphisms in SARS-CoV-2 RNA-dependent RNA polymerase on its activity and sensitivity to inhibitors *in vitro*, *Biochimie*, **206**, 81-88, https://doi.org/10.1016/j.biochi.2022.10.007.

39. Matyugina, E., Petushkov, I., Surzhikov, S., Kezin, V., Maslova, A., Ivanova, O., Smirnova, O., Kirillov, I., Fedyakina, I., Kulbachinskiy, A., Kochetkov, S., and Khandazhinskaya, A. (2023) Nucleoside analogs that inhibit SARS-CoV-2 replication by blocking interaction of virus polymerase with RNA, *Int. J. Mol. Sci.*, **24**, 3361, https://doi.org/10.3390/ijms24043361.

40. Zhilina, E., Miropolskaya, N., Bass, I., Brodolin, K., and Kulbachinskiy, A. (2011) Characteristics of sigma-dependent pausing in RNA polymerases from *E. coli* and *T. aquaticus*, *Biochemistry (Moscow)*, **76**, 1348-1358, https://doi.org/10.1134/S0006297911100038.

41. Zhilina, E., Esyunina, D., Brodolin, K., and Kulbachinskiy, A. (2012) Structural transitions in the transcription elongation complexes of bacterial RNA polymerase during sigma-dependent pausing, *Nucleic Acids Res.*, **40**, 3078-3091, https://doi.org/10.1093/nar/gkr1158.

42. Petushkov, I., Esyunina, D., and Kulbachinskiy, A. (2017) sigma38-dependent promoter-proximal pausing by bacterial RNA polymerase, *Nucleic Acids Res.*, **45**, 3006-3016, https://doi.org/10.1093/nar/gkw1213.

43. Leonard, G. A., Guy, A., Brown, T., Teoule, R., and Hunter, W. N. (1992) Conformation of guanine-8-oxoadenine base pairs in the crystal structure of d(CGCGAATT(O8A)GCG), *Biochemistry*, **31**, 8415-8420, https://doi.org/10.1021/bi00151a004.

44. Arnold, J. J., and Cameron, C. E. (2004) Poliovirus RNA-dependent RNA polymerase (3Dpol): pre-steady-state kinetic analysis of ribonucleotide incorporation in the presence of Mg^{2+}, *Biochemistry*, **43**, 5126-5137, https://doi.org/10.1021/bi035212y.

45. Arnold, J. J., Gohara, D. W., and Cameron, C. E. (2004) Poliovirus RNA-dependent RNA polymerase (3Dpol): pre-steady-state kinetic analysis of ribonucleotide incorporation in the presence of Mn^{2+}, *Biochemistry*, **43**, 5138-5148, https://doi.org/10.1021/bi035213q.

46. Huang, Y., Beaudry, A., McSwiggen, J., and Sousa, R. (1997) Determinants of ribose specificity in RNA polymerization: effects of Mn^{2+} and deoxynucleoside monophosphate incorporation into transcripts, *Biochemistry*, **36**, 13718-13728, https://doi.org/10.1021/bi971609o.

47. Ranjith-Kumar, C. T., Kim, Y. C., Gutshall, L., Silverman, C., Khandekar, S., Sarisky, R. T., and Kao, C. C. (2002) Mechanism of de novo initiation by the hepatitis C virus RNA-dependent RNA polymerase: role of divalent metals, *J. Virol.*, **76**, 12513-12525, https://doi.org/10.1128/jvi.76.24.12513-12525.2002.

48. Te Velthuis, A. J. W., Arnold, J. J., Cameron, C. E., van den Worm, S. H. E., and Snijder, E. J. (2009) The RNA polymerase activity of SARS-coronavirus nsp12 is primer dependent, *Nucleic Acids Res.*, **38**, 203-214, https://doi.org/10.1093/nar/gkp904.

49. Gottesman, M. E., Chudaev, M., and Mustaev, A. (2020) Key features of magnesium that underpin its role as the major ion for electrophilic biocatalysis, *FEBS J.*, **287**, 5439-5463, https://doi.org/10.1111/febs.15318.

50. Poranen, M. M., Salgado, P. S., Koivunen, M. R. L., Wright, S., Bamford, D. H., Stuart, D. I., and Grimes, J. M. (2008) Structural explanation for the role of Mn^{2+} in the activity of ϕ6 RNA-dependent RNA polymerase, *Nucleic Acids Res.*, **36**, 6633-6644, https://doi.org/10.1093/nar/gkn632.

51. Vassylyev, D. G., Vassylyeva, M. N., Zhang, J., Palangat, M., Artsimovitch, I., and Landick, R. (2007) Structural basis for substrate loading in bacterial RNA polymerase, *Nature*, **448**, 163-168, https://doi.org/10.1038/nature05931.